Journal of Power Sources 213 (2012) 391–401

Contents lists available at SciVerse ScienceDirect

Journal of Power Sources

journal homepage: www.elsevier.com/locate/jpowsour

Modelling the impact of variations in electrode manufacturing on lithium-ion battery modules

Ben Kenney, Ken Darcovich*, Dean D. MacNeil, Isobel J. Davidson

NRC Energy, Mining and Environment Portfolio, National Research Council Canada, Ottawa, Ontario, Canada K1A 0R6[1]

ARTICLE INFO

Article history:
Received 25 January 2012
Received in revised form
20 March 2012
Accepted 21 March 2012
Available online 13 April 2012

Keywords:
Lithium-ion battery
Electrode variability
Degradation
Battery modules
Battery packs

ABSTRACT

The performance of a lithium-ion battery is closely related to its manufacturing and can be impacted by variability in the electrodes. Typically, manufacturers must set aside cells which are deemed to be of insufficient quality, thus contributing to the cost of manufacturing high quality cells. The performance of a lithium-ion battery module, that is, a string of cells configured in series, depends on the performance of the weakest cell. In this work, the single particle model was adapted to simulate the coupled behaviour of an arbitrary number of cells configured in series. The impact of slight variations in the manufacturing of electrodes was then investigated with a goal of linking electrode properties such as variations in thickness, electrode density and active material weight fraction with the performance of battery modules made from these cells. Results indicate that the initial capacity, the rate of capacity fade and other important aspects such as the distribution of state-of-charge from one cell to another depends on the extent of variability in the manufacturing of the electrodes. In this work, the variation in the performance of the module has been quantified as a function of manufacturing variation at the electrode level.

1. Introduction

Lithium-ion batteries are currently the preferred technology for the electrification of vehicles on account of their high energy and power densities. Like many electrochemical technologies, the cost of lithium-ion batteries must be reduced for wide scale commercial adoption. The task of reducing the cost of lithium-ion batteries falls on researchers for inventing new, higher capacity materials or better electrode designs tailored for specific applications, as well as on cell manufacturers who must control manufacturing tolerances of individual cells to precise levels to maximize the performance and lifetime of a battery pack, which can consist of hundreds or thousands of individual lithium-ion battery cells.

The manufacturing of lithium-ion cells, starting from commercial active material and additive materials involves mixing the electrode slurry in the correct proportions for a specific application, casting of the electrode slurry, usually onto aluminium or copper foils, calendering of the casts to compress the electrodes to achieve a desired electrode density or porosity and finally assembling the cell components. In each manufacturing stage, there exists a certain tolerance which must be met in order to produce high quality, viable cells that pass quality control measures.

A battery pack typically consists of groups of modules which themselves are made up of many cells configured in series. For battery modules, each of its cells is subjected to the same current, and its voltage is the sum of the individual cell voltages. The battery management system must ensure that operating limits on each cell are observed, and therefore the capacity of the battery module is limited to the capacity of the weakest cell within the module. For this reason, small cell-to-cell variations arising from the manufacturing stage may result in significant variations to the overall electrochemistry and capacity of the battery pack. The link between cell manufacturing variations and their overall impact on a full battery module or pack can be difficult and expensive to establish. In this work, we have used mathematical modelling techniques to predict how these cell-to-cell variations manifest thermselves in an operational battery module.

* Corresponding author. Tel.: +1 613 993 6848; fax: +1 613 991 2384.
E-mail address: ken.darcovich@nrc-cnrc.gc.ca (K. Darcovich).
[1] NRCC No. 53060.

0378-7753/$ – see front matter
doi:10.1016/j.jpowsour.2012.03.065

Mathematical modelling can play an important role when designing individual cells and also when scaling up to larger systems. Models involving detailed coupled electrochemical processes exist [1–11], as well as simplifications to the fully coupled electrochemical model, such as the single particle model [12–17] as well as resistor based models, recently reviewed in [18]. To date, most physics-based models have focused on predicting the performance of an individual cell and battery pack modelling has been done either by considering only a single cell and ignoring any cell-to-cell differences [19] or by using resistor based models that simulate the lithium-ion battery pack or module [20,21]. While resistor based models can obtain fast solutions, they cannot be used in a predictive capacity since they are not physics-based and the parameters are specific to an individual cell. Recently, it has been shown that the single particle model [14] can be used to replace resistor based models in the prediction of individual cells. The adavantage of the single particle model is that it is derived based on simplifications to the full electrochemical model and therefore it is physics-based, but the time required to solve its equations are on the same time scale as a resistor based model. In addition, phenomena such as degradation kinetics and SEI formation can be incorporated into the single particle model so that the initial capacity of the cell can be modelled as well as capacity of the cell for any subsequent cycle.

In this work, we have extended the single particle model to simulate lithium-ion battery modules consisting of an arbitrary number of cells configured in series. With this new physics-based simulation tool for battery modules, we estimate how variations in the manufacturing of the electrodes in the individual cells that make up the battery pack can influence the overal capacity, degradation and electrochemistry of the pack. The objective is to identify which manufacturing steps, from the mixing of active material and additives, the casting of electrodes and the calendaring of the electrodes, require strict quality control and to what level so optimal performance from high performance battery packs can be achieved.

2. Mathematical model

A description of the single particle model is available in Refs [12–16]. The single particle model assumes that the majority of the cell polarization is attributed to the lithium diffusion in the active material particle and the kinetics of the charge transfer reaction. In such circumstances, the gradient in the electrolyte concentration and ionic phase potential can be assumed to be negligible, allowing for spatial distributions along the cell thickness to be ignored. As a consequence, any distribution in porosity and tortuosity is also assumed to be negligible since these would primarily influence the effective diffusion coefficient and effective ionic conductivity of the electrolyte. However, the porosity is accounted for in the calculation of the active surface area of the electrodes. These assumptions become increasingly valid as the current through the cell approaches zero. Commonly, the single particle model is used for currents less than 1C but it has been used succesfully in situations involving HPPC pulses up to 5C [17] assuming an appropriate solution method for the solid phase lithium diffusion equation. In this work, the maximum applied current was 0.8 A, roughly C/3. Under these conditions, the ohmic resistance, inveserly proportional to the effective ionic conductivity and proportional to the cell thickness, was found to be neglible. In addition, by virtue of the low currents, we assumed an isothermal system since it has been reported that the temperature is mostly constant for currents as low as C/3 [22,23].

2.1. Theory/model development

In a lithium-ion battery, lithium is stored or removed from the active cathode and anode materials by diffusing through spherical electrode particles. This intercalation step is driven by the intercalation current and can be described by a transient spherical diffusion equation:

$$\frac{\partial c_i}{\partial t} = \frac{D_i}{r^2}\frac{\partial}{\partial r}\left(r^2\frac{\partial c_i}{\partial r}\right) \quad i = (\text{pos}, \text{neg}) \tag{1}$$

where c_i is the concentration of lithium inside the spherical particle, r is the radial position inside the spherical particle and D_i is the solid phase diffusion coefficient in electrode i (either positive or negative). Eq. 1 has boundary conditions:

$$D_i\frac{\partial c_i}{dr} = -J_i \quad \text{at} \quad r = R_p \tag{2}$$

$$\frac{\partial c_i}{dr} = 0 \quad \text{at} \quad r = 0 \tag{3}$$

where J_i is the intercalation current density at the surface of the particle, described by Butler–Volmer kinetics:

$$J_i = i_{0,i}\left[\exp\left(\frac{\alpha F}{RT}\eta_i\right) - \exp\left(\frac{-\alpha F}{RT}\eta_i\right)\right] \tag{4}$$

and the exchange current density is

$$i_{0,i} = Fk_{ct,i}(C_{max,i} - \theta_i C_{max,i})^{0.5}(\theta_i C_{max,i})^{0.5}C_e^{0.5} \tag{5}$$

where k_{ct} is the rate of the electrochemical reaction, C_{max} is the maximum concentration of lithium that can be stored in the active material, θ is the state-of-charge of the electrode and C_e is the concentration of lithium salt (1000 mol m^{-3}).

The intercalation current density is related to the applied current and the internal surface area of the electrode (S_i): $J_i = I_{tot}/S_i$. With this definition, the electrode overpotential, η_i, can be solved in Eq. 4 to calculate the electrode potentials:

$$\phi_{1,i} = \eta_i + \phi_2 + E_{ref,i} + J_i R_{film,i} \tag{6}$$

where $R_{film,i}$ is the film resistance on the electrode particle, and $E_{ref,i}$ is the reference potential of the electrode. Subscript i refers to either the positive or negative electrodes.

The cell voltage is then simply defined as the difference between the positive and negative electronic phase potentials:

$$V = \phi_{1,p} - \phi_{1,n} \tag{7}$$

To simulate constant voltage charging in a CCCV charge protocol, an iterative process was used to find the correct current density such that the voltage remained at the specified level.

The influence of an ohmic drop, $\phi_{2,pos} - \phi_{2,neg}$, can be estimated based on the effective ionic conductivity of the electrolyte and the thickness of the electrodes and separator:

$$I_{tot}R_{ohmic} = \frac{I_{tot}}{A} \times \left(\frac{L_{pos}}{\sigma_{ion}\varepsilon_{pos}^{brugg}} + \frac{L_{sep}}{\sigma_{ion}\varepsilon_{sep}^{brugg}} + \frac{L_{neg}}{\sigma_{ion}\varepsilon_{neg}^{brugg}}\right) \tag{8}$$

where σ_{ion} is the ionic conductivity of the electrolyte, and brugg is the Bruggeman factor ~1.5. Using Eq. 8, it is easy to show that the the potential drop due to the Ohmic resistance is negligible at a rate of C/3 and the term $\phi_{2,pos} - \phi_{2,neg}$ is commonly excluded from the single particle model.

A side reaction which consumes a portion of the intercalation current in the anode, forming an SEI layer, was also considered. To simplify parameter estimation, the details of the elementary reactions that make up the SEI film formation reaction mechanism, recently modelled by Colclasure et al. [24], have not been considered. Instead, the mechanism was simplified to a single reaction similar to that reported in Refs [8,12,14]. Although secondary and tertiary degradation mechanisms have been ignored, this side reaction has been validated against commerical lithium-ion cells for up to 1968 cycles [8]. During cell charging, lithium is inserted into the anode particles, however, a side reaction reduces ethylene carbonate (EC) to form lithium carbonate. This side reaction siphons a portion of the intercalation current and deposits the by-product onto the active particle surface of the anode. This reaction is considered to be an irreversible electrochemical reduction reaction and can be expressed by

$$S + 2Li^+ + 2e^- \rightarrow P \tag{9}$$

where S refers to the solvent and P is the side reaction product. In such a case, the intercalation current density at the anode is decreased due to the side reaction current density, and becomes:

$$J_{neg} = \frac{I_{tot}}{S_{neg}} - J_s \tag{10}$$

where J_s is the side reaction current, calculated from a Tafel approximation of the Butler–Volmer equation:

$$J_s = -i_{0s}\exp\left(\frac{-\alpha_c F}{RT}\eta_s\right) \tag{11}$$

As EC is reduced and the side reaction proceeds, both the thickness of the SEI layer and its resistance increase according to:

$$\frac{dL_{SEI}}{dt} = \frac{-J_s M_p}{\rho_p F} \tag{12a}$$

$$R_{SEI} = \frac{L^0_{SEI}}{\kappa_p} + \frac{L_{SEI}}{\kappa_p} \tag{12b}$$

where M_p, ρ_p and κ_p are the molar mass, density and electronic conductivity of the product film and L^0_{SEI} is the initial film thickess. As a result of the parasitic side reaction, less lithium is available to be stored in the particles and the resistance of the SEI layer increases.

After the charge cycle, the lost capacity of the cell, Q_s and the lost SOC, θ_s, can be calculated by:

$$Q_s = -\int_{t=ch.start}^{t=ch.end} S_{neg} J_s dt \tag{13a}$$

$$\theta_s = \frac{Q_s}{Q_{max}} \tag{13b}$$

where Q_{max} is the rated capacity of the cell (or the capacity of the first cycle). To start the next cycle, the SOC of the positive electrode is updated to reflect the new starting condition where $\theta^0_p = \theta^0_p|_{N-1} - \theta_s|_{N-1}$.

The above equations apply to a single lithium-ion cell and were programmed using Python and the Scipy [25] and Numpy numerical libraries. Eq. 1 is a partial differential equation and although algebraic approximations exist, we chose to use the full finite difference solution method.

2.2. Battery module simulation

Under single cell operation, the equations can be solved at successive time steps, however, some extra consideration must be given for the simulation of cells configured in series, especially if the model is to simulate multiple cycles of the battery pack. This solution algorithm is given in Fig. 1. In a series configuration assuming negligible losses in the current collectors, the current through each cell is the same and the capacity of the battery pack is limited to that of the weakest cell in the series. The voltage at each time step is simply the sum of the voltages of the individual cells:

$$V_{pack}(t) = \sum_{cell=1}^{n} V_{cell}(t) \tag{14}$$

For each time step, the equations describing the cell behaviour must be solved sequentially for each cell in the series. During discharge, the simulations are marched forward in time until one cell in the series hits the low voltage cutoff, such as 2.5 V, at which point, the current flowing through the cells must be changed to a charging current so as to not over-discharge the cells, causing potentially dangerous operation of the battery pack. In this work, we have considered a cell balancing technique for the charging of cells. The charging starts with a standard constant current charge until each cell hits the voltage cutoff of 4.2 V, at which point, each cell undergoes an independent constant voltage charging mode until the maximum current flowing through the cells has diminished to less than or equal to 50mA. This type of charging behaviour is similar to the cell balancing of a battery management system

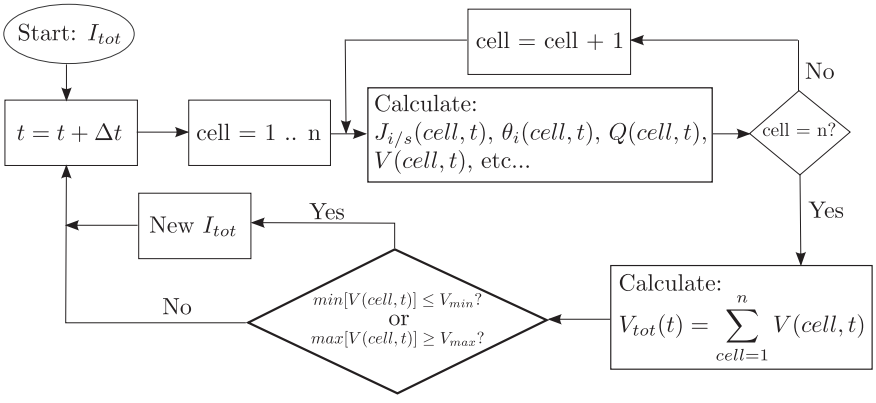

Fig. 1. Simulation algorithm for cells in series. The electrochemistry of each cell is simulated individually and an algorithm was used to control the end-of-discharge/charge to ensure that each cell stayed within its voltage window.

accomplished by bleeding each cell to maintain a constant 4.2 V and ensuring that individual cells are fully charged. Depending on the cell-to-cell variability, this may mean that some cells are maintained at 4.2 V longer than others.

2.3. Model parameters

The model parameters include kinetic, transport and geometrical parameters. The kinetic and transport parameters are independent of the electrode's microstructure and were determined for each individual electrode by fitting the parameters against low rate experimental cycle data of a commercial 18650 cell with $LiCoO_2$ (LCO) cathode and graphite anode. These parameters compared favourably to those found in the literature for the same material Ref [12]. The geometrical parameters of the electrodes were determined by dissasembling the 18650 cell and measuring the thicknesses and geometric areas of the electrodes. This process was complicated by the fact that the electrode material had laminated to the separator making accurate thickness measurements difficult. The thicknesses were then estimated based on these measurements and compared against the findings of commercial cells from Johnson and White [26].

In addition to the kinetic and transport parameters, we also estimated the side reaction exchange current density, i_{0s} with data on the capacity fade of 200 cycles of the 18650 cell. We then used this i_{0s} to predict the cycling behaviour to 1000 cycles.

Overall, the kinetic and transport parameters which were fit against experimental data included:

- The electrochemical rate constant for cathode and anode, $k_{ct,i}$
- The lithium diffusion coefficient in the active material for cathode and anode, D_i
- The side reaction exchange current density of the anode, i_{0s}

Because the kinetic and transport parameters are microstructure independent, predictions using these parameters and varying design parameters can then be made. Given an electrode thickness, electrode density, particle size and weight fractions of the active material (AM), binder (B) and carbon conductor (C), important parameters such as the electrode porosity (ε_i) and the internal surface area (S_i) can be calculated using the following relationships:

$$\varepsilon_i = 1 - \frac{\rho_i^{eode}}{\rho_i^{bulk}} \quad i = (\text{pos}, \text{neg}) \tag{15a}$$

$$S_i = \frac{3V_{AM,i}(1-\varepsilon_i)}{R_{p,i}} \quad i = (\text{pos}, \text{neg}) \tag{15b}$$

$$\rho_i^{eode} = \sum_{j=AM,C,B} \rho_j V_{j,i} \quad i = (\text{pos}, \text{neg}) \tag{15c}$$

$$V_j = \frac{w_j}{\rho_j} \times \left[\sum_{k=AM,C,B} w_k/\rho_k \right]^{-1} \quad j = (\text{AM}, \text{C}, \text{B}) \tag{15d}$$

In the above equations, ρ_i^{eode} is the density of the electrode (either positive or negative), ρ_i^{bulk} is the density of the bulk electrode (the electrode density based on each of its components but assuming no porosity), V_j is the volume fraction of component j in the electrode, and ρ_j is the density of component j. The electrode components include: the active material (AM), carbon filler (C) and the binder material (B). During the manufacturing stage of an electrode, the electrode density can be controlled in a number of ways, such as by varying the amount of NMP/solvent or weight fraction of active material (w_{AM}) during the casting of the electrode slurry, by the evaporation rate of NMP in the cast or by the pressure used in the calendering process. In addition to these kinetic and transport parameters, open circuit voltage (OCV) curves for the individucal LCO and graphite electrodes were required. This data has been previously reported [14] for the LCO and graphite electrodes respectively and Eqs. 16 and 17 are curve fit expressions for LCO cathode and graphite anode respectively:

$$E_{ref,p}(\theta_p) = \frac{-4.656 + 88.669\theta_p^2 - 401.119\theta_p^4 + 342.909\theta_p^6 - 462.471\theta_p^8 + 433.434\theta_p^{10}}{-1 + 18.933\theta_p^2 - 79.532\theta_p^4 + 37.311\theta_p^6 - 73.083\theta_p^8 + 95.96\theta_p^{10}} \tag{16}$$

$$E_{ref,n}(\theta_n) = 0.7222 + 0.1387\theta_n + 0.029\theta_n^{0.5} - \frac{0.0172}{\theta_n} + \frac{0.0019}{\theta_n^{1.5}} + 0.2808\exp(0.9 - 15\theta_n) - 0.7984\exp(0.4465\theta_n - 0.4108) \tag{17}$$

2.4. Modeling procedure

The purpose of this study was to investigate how tolerances that may exist in the electrode fabrication process of lithium-ion cells impact the overall performance of a battery pack. The three main electrode fabrication parameters studied were: 1) The electrode thickness 2) The electrode density, related to the porosity of the electrode, and 3) The weight fraction of active material, related to the quality of mixing of the active material with conductive agents and binders. For each of these three parameters, it was assumed that a small variation at the manufacturing level existed and that

Table 1
The range of manufacturing tolerances simulated in this work. The standard deviations listed here are those that make up the normal distributions shown in Fig. 2(a) and (b).

Parameter	Description	Standard deviation		
		Low	Med	High
L	Electrode thickness	±1%	±2%	±5%
ρ^{eode}	Electrode density	±1%	±2%	±5%
w_{AM}	Weight fraction of active material	±0.1%	±0.2%	±0.5%

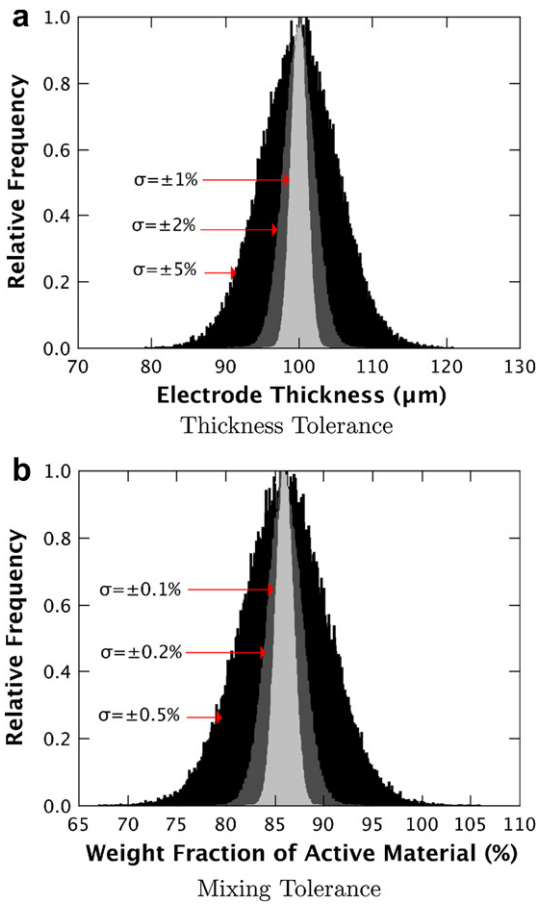

Fig. 2. Example of (a) Variation of electrode thickness with 1%, 2% and 5% standard deviation (b) Variation of active material in electrode with 0.1%, 0.2% and 0.5% standard deviation.

the variation fell within a normal distribution. The simulations assumed variations for both the thickness and the electrode density were ±1%, ±2% and ±5% of the mean while the variations on the weight fraction of active materials were ±0.1%, ±0.2% and ±0.5% of the mean. Since manufacturing variations are not published by battery manufacturers, we chose a range which we judged to be reasonable for the variation of each parameter based on the experimental work that has previously been done in our lab fabricating various electrodes for coin cells [27–29]. Unless otherwise stated, these variations are denoted qualitatively as low, med and high, as shown in Table 1.

For the majority of this work, battery modules consisting of 15-cells configured in series were simulated at a discharge current of −0.8 A (approximately C/3). The manufacturing parameters for each cell were randomly chosen within the normal distribution for that parameter. Fig. 2(a) and (b) show examples of the distributions of the cathode thickness and the weight fraction of the cathode active material from which the cell parameters were randomly selected. Since each pack consisted of 15-cells with randomly selected parameters, numerous battery modules were simulated in order to obtain mean and standard deviations on the module capacities which were fabricated from the same batch of cells. This is equivalent to the physical scenario of battery modules being made from a batch of cells fabricated with the same manufacturing tolerances. For this study, 130 modules were simulated and averaged to provide the upper and lower capacity range for each set of parameter tolerances.

3. Experimental

Commercial 18650 cells made from LCO cathode and graphite anodes were cycled at room temperature on an Arbin cycler between 4.2 and 2.5 V. The capacity of the cells were determined by first cycling at very low currents, followed by a C/12 charge and discharge over 5 cycles to condition the cell. To verify the model against experimental data, a cycle routine consisting of C/12, C/9, C/6 and C/3 discharge with C/3 and constant voltage charge protocol was used. After these initial cycles, the cell was cycled over 200 cycles at C/3 with the rate capability verified every 10 cycles between 1C and C/50. Once the cell cycling had finished, the 18650 cell was dissasembled by cutting and removing the canister and unrolling the electrodes to measure physical parameters such as the electrode thickness and the geometric area. For these cells, the geometric area was 0.07m^2 and the cathode and anode thicknesses were estimated to be 100 and 105 microns respectively.

4. Results and discussion

4.1. Single cell parameter fitting

Experimental data was used to validate the model for a single LCO | graphite cell. After the initial cell conditioning phase, model parameters were estimated based on discharge cycles between C/12 and C/3 with a CCCV charge protocol and a 50mA cutoff current. These experiments provided estimates of the insertion reaction's electrochemical kinetic rate constants as well as the solid phase diffusion coefficients. The exchange current density of the side reaction, i_{0s}, was estimated separately based on the capacity fade of the experimental cell over 200 cycles at a rate of C/3. Table 2 outlines the parameters used in this study while Fig. 3(a) shows the resulting model fit against the experimental data for the discharge cycles and Fig. 3(b) shows the model fit of the capacity fade. The starting parameter estimates for the kinetic and transport parameters were taken from Ning and Popov [12] and then further refined for the collected experimental data. The normalized mean square error (Eq. 18) of the parameter fit was 0.46 for Fig. 3(a) and 0.02 for Fig. 3(b).

$$\text{nmse} = \frac{\text{mean}\left[(\text{exp} - \text{mod})^2\right]}{\text{var}(\text{exp})} \tag{18}$$

4.2. Simulation of ideal lithium-ion battery module

A battery module is defined as a string of single cells configured in series. When each cell within a battery module is identical

Table 2
List of model kinetic, transport and geometrical parameters.

Parameter	Pos value	Neg value	Units	Source
k_{ct}	1.27×10^{-12}	1.67×10^{-12}	$m^{2.5}\ s^{-1}\ mol^{0.5}$	Fit
D_s	1×10^{-13}	3.8×10^{-14}	$m^2\ s^{-1}$	[12]
i_{0s}	–	3.2×10^{-8}	$A\ m^{-2}$	Fit
L^a	100	105	μm	Measured and [26]
Q	274.64	363.0	$mAh\ g^{-1}$	Calculated
A	0.07	0.07	m^2	Measured
R_p	5	6	μm	Assumed
$\rho^{eode,a}$	3.07	1.24	$g\ cm^{-3}$	Measured and [26]
$w_{AM}{}^a$	86	96	%	Assumed and [26]
M_p	–	0.1	$kg\ mol^{-1}$	[12]
ρ_p	–	2100	$kg\ m^{-3}$	[12]
κ_p	–	5×10^{-6}	$S\ m^{-1}$	[12]
$E_{ref,s}$	–	0.4	V	[12]
T	298	298	K	–

[a] These represent the mean values and are varied for parts of this work

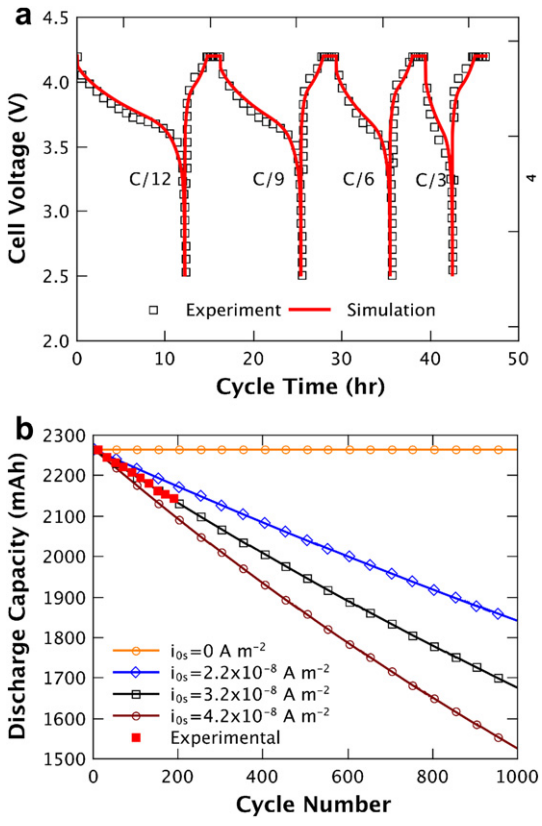

Fig. 3. (a) Model fit against experimentally collected discharge (from C/12 to C/3) and CCCV charge curves (C/3 charge and 50 mA cutoff) in an 18650 cell (b) Model fit against the capacity fade of an 18650 cell.

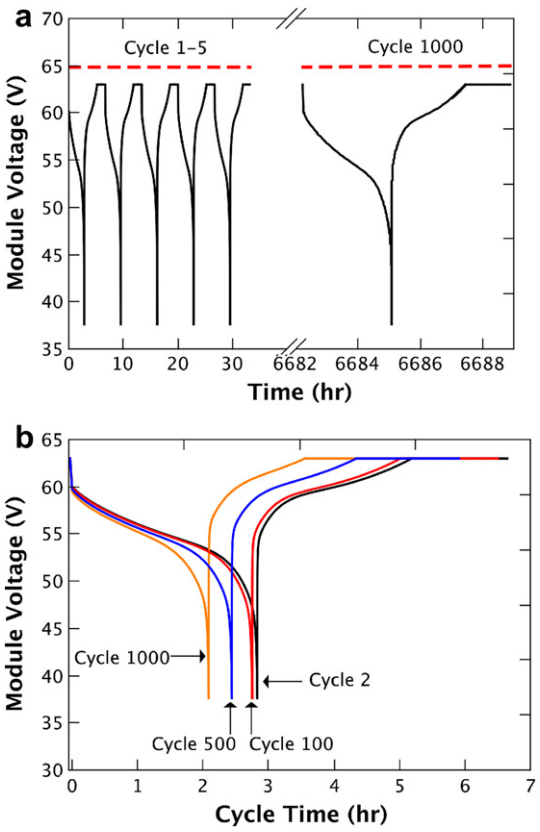

Fig. 4. (a) Cycle behaviour and (b) comparison of capacity fade of a 15-cell module with no cell-to-cell variation at a discharge current of −0.8 A (approximately C/3).

to one another, meaning not just identical capacities but also identical electrode microstructures, each cell and electrode within the module is exposed to the same intercalation current and maintains an identical voltage profile to one another throughout the lifetime of the module. Given this type of hypothetical module, the capacity of the module would be equivalent to the capacity of a single cell. The voltage of the module is additive and follows Eq. 14.

Fig. 4(a) and (b) show the typical cycling behaviour of an ideal lithium-ion battery module. While each cell within the module cycles between a high and low voltage of 4.2 V and 2.5 V, as shown by the single cell cycles in Fig. 3(a), the module cycles between a high voltage limit of 4.2 V×15 cells = 63 V and a low voltage limit of 2.5 V×15 cells = 37.5 V. Each cell that makes up this module has exactly the same cycle behaviour. The output gives identical state-of-charge and capacity fade curve which are determined by the parameters that were found to fit the experimental data in Fig. 10.

The capacity fade of the module, shown in Fig. 4(b), represents a 26.2% reduction in the capacity of the cells over 1000 cycles, from 2.26 Ah to 1.67 Ah. After the constant current charge step of cycle 2, the charge capacity of each cell was 1.89 Ah and the constant voltage charge topped up the charge capacity by 0.378 Ah, whereas after cycle 1000, the constant current charge capacity was reduced to 1.18 Ah and the constant voltage portion added an additional 0.494 Ah. At the same time, the internal resistance of the cells increased over the 1000 cycles due to the build-up of SEI on the anode particles, growing from a resistance of 0.02Ωm^2 to 0.076Ωm^2 on a surface area basis.

It is important to note that due to the coupling of transport and electrochemical processes in the battery with the cell's electrode microstructure, even the slightest variations in the manufacturing of electrodes, ultimately resulting in variations in the electrode microstructure, results in cell-to-cell differences in charge times, state-of-charge and SEI/cell degradation. A mathematical description of how electrode manufacturing variations can influence the electrode microstructure was given by Eq. 15. Variations in thickness, apparent electrode density and active material fraction influence the internal surface area, porosity and volume fractions of the electrode which in turn influence various transport and electrochemical processes. These variations in individual cells influences the performance of the battery module as a whole and the impact of these manufacturing variations are discussed below.

4.3. Influence of electrode manufacturing variations on battery performance

4.3.1. Simulation of individual cells

During the production of lithium-ion cells, many factors can influence the performance of an individual cell, from electrode manufacturing to cell assembly. For the electrode manufacturing stage, factors related to the quality of the electrode slurry, the roll-to-roll casting of the slurry onto aluminium or copper foil and the drying and calendering process could result in individual cells having slight variations in their electrode microstructures.

Due to the coupled nature of electrochemical processes, the impact of small variations caused by manufacturing processes can be difficult to ascertain without mathematical modelling. Fig. 5 shows the distribution of the single cell capacities after cycle 2 and cycle 1000 resulting from "low" and "high" variations in

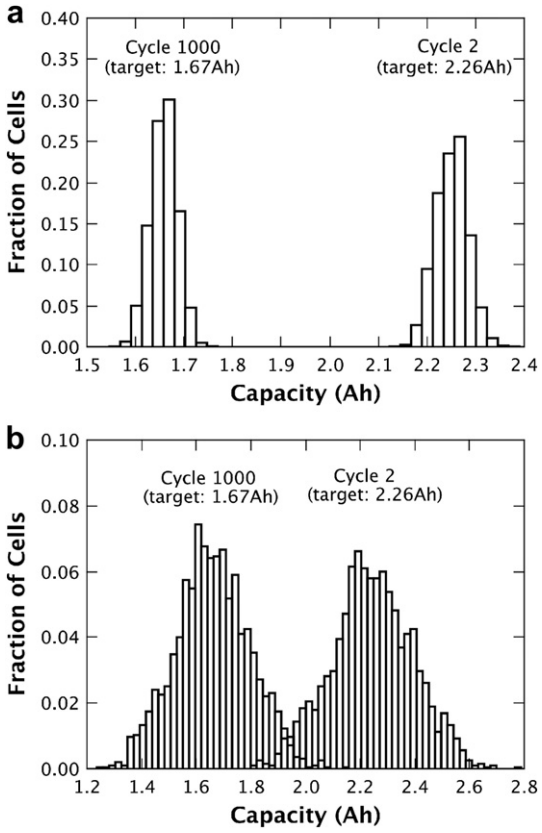

Fig. 5. Single cell capacity distribution for all the cells that make up the 130 15-cell modules a) low variation in all manufacturing parameters b) high variation in all manufacturing parameters. The low and high parameter variations are outlined in Table 1. The bin size was chosen to represent 1% variance around the target capacity, which was 2.26 Ah. The discharge current was -0.8 A.

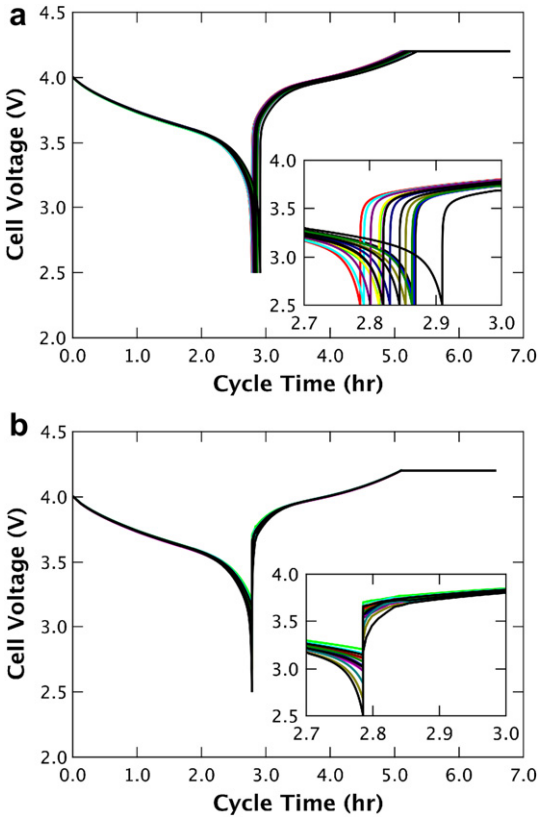

Fig. 6. (a) Discharge curves (cycle 2) of single cells making up a module (b) The behaviour of those same cells while configured in the module. Inset shows the same data near the end of the discharge. Simulations were performed using low manufacturing variabilities on all parameters with a discharge current of −0.8 A.

electrode manufacturing, as outlined in Table 1. These figures represent a batch of 1950 individual cells whose parameter sets were also used to simulate 130 individual 15-cell battery modules. These large sample sizes were required for statistical resolution since the manufacturing parameters were selected randomly from the normal distributions shown in Fig. 2(a) and (b). As can be expected, the spread in the capacities of the individual cells increase as the variation in manufacturing increases. For example, Fig. 5(a) shows the range of capacities in single cells associated with a low variation in the electrode thickness, apparent electrode density and active material weight fraction. The difference in capacity between the highest and lowest capacity cells from this batch was 0.246 Ah whereas the target capacity, had there been no manufacturing variations, was 2.26 Ah, making the differential about 10% of the target capacity. Each bar in Fig. 5 represents a 1% capacity differential, which means that if a module was to be built from this batch of cells and the target capacity of the module was 2.26 Ah ± 1%, then only 25% of the cells could be used (assuming the higher capacity cells were used for other purposes). This outlines the importance of keeping tight control over the manufacturing process of the individual electrodes since a large portion of cells would have to be discarded to ensure good performance of the battery module. Fig. 5(b) shows similar results except for high variation in manufacturing. In this case, the difference between high and low initial capacities is 1 Ah and the fraction of cells that can be used to build a module with a specified capacity drops by more than a factor of three.

Typically, a battery module is constructed from a batch of single cells that are chosen to have matching capacities within some specified capacity range. This late stage quality control results in some cells being classified as high quality while others are low quality, influencing the cost of the cells. For this reason, it is important to understand some of the factors associated with this variance in capacity and how these variations may ultimately impact a battery module. It is the intention of this work to establish a more direct link between the variation in the electrode manufacturing with the final capacity of modules assembled from those cells.

4.3.2. Simulation of 15-cell battery modules

The simulation of a battery module assembled with identical cells configured in series is relatively straightforward assuming the cells remain perfectly balanced throughout their lifetime. In such a case, only a single cell needs to be simulated and the voltage of the battery module can be calculated using Eq. 14 and the capacity of the module is simply the capacity of an individual cell. However, if the cells become unbalanced, due to defects in the electrodes which may arise from variations in the manufacturing stage, the battery management system must work to ensure that each cell remains within a specified voltage window for safe operation. During discharge, slight variations in electrode manufacturing can result in some cells within the module reaching 2.5 V before others. In this case, the module must be treated as fully discharged, despite some cells having further capacity. In the model outlined in Section 2.1 and 2.2, an algorithm was developed allowing battery modules to be simulated by coupling the charge and discharge behaviour of individual cells within the module in the same way that a battery

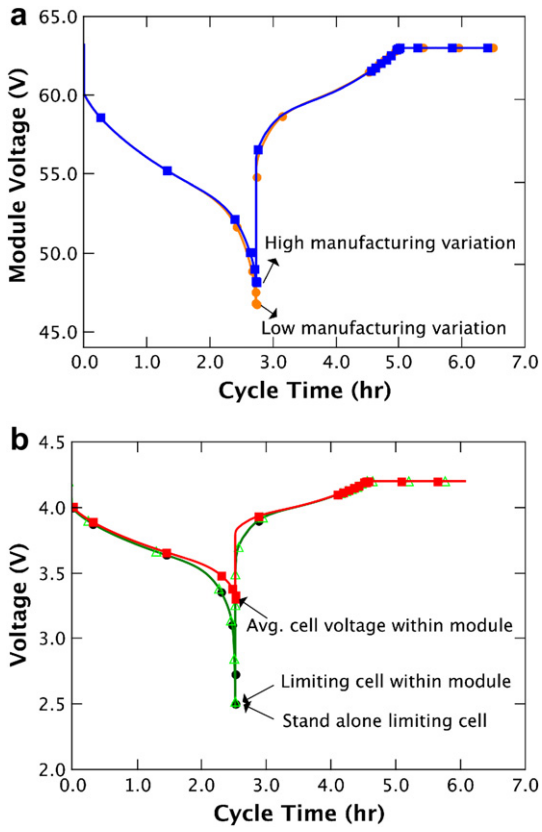

Fig. 7. (a) Module discharge and charge profiles for low and high manufacturing variations selected for a case where the capacity of the two modules was the same (2.18 Ah) (b) Comparison of the average discharge and charge profiles of cells within a module against the discharge and charge profiles of the limiting cell simulated on its own as well as within a module configuration.

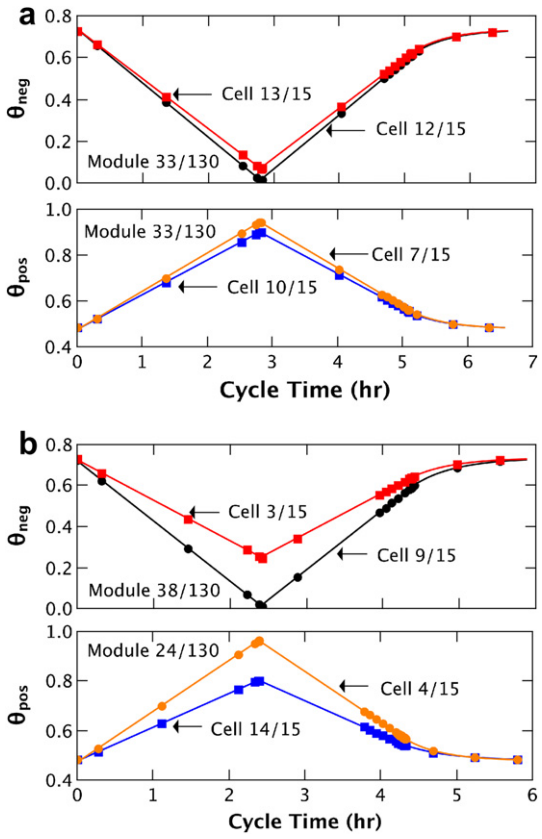

Fig. 8. Maximum and miniumum lithiation in positive and negative electrodes during cycle 2 for (a) low variation in all parameters and (b) high variation in all parameters. The data represent the modules (out of the 130 which were simulated) that exhibited the maximum spread in lithiation between individual cells.

management system would ensure safe operating voltages of each cell. This algorithm is important when it comes to simulating modules that are built with slight variations between individual cells, since the behaviour of cells within a module is not necessarily equivalent to the behaviour of a single cell. Fig. 6(a) and (b) depicts the differences between cell behaviour simulated individually and while configured in a module with low manufacturing variations. The inset figures represent the same data but are focused around the end-of-discharge for these two situations.

When tested or simulated as single cells, Fig. 6(a) shows that each cell is allowed to discharge completely before the charge cycle begins. Slight variations in the manufacturing stage of the cell result in slight capacity differences and internal resistances due to factors such as thickness, electrode density and differences in the fraction of active material, producing capacities of ranging from a high of 2.33 Ah to a low of 2.23 Ah with an average of 2.26 Ah. By comparison, Fig. 6(b) shows the behaviour of the same cells but configured in a module. The spread in discharge and charge curves is much lower for these cells configured in a module because the capacity and state-of-charge of each cell is limited to prevent over-discharge or over-charge. The capacity of the module is limited by the weakest cell within the module, in this case, the cell with the capacity of 2.23 Ah.

As a result of the distribution in end-of-discharge voltages observed in Fig. 6(b), cycling individual cells between 4.2 V and 2.5 V within a module of unbalanced cells does not correspond to an end-of-discharge module voltage of 2.5 V $\times$ 15 $=$ 37.5 V but instead to a higher end-of-discharge module voltage. Fig. 7(a) shows an example of the discharge curves of two 15-cell modules simulated with the assumption of low and high manufacturing variations and matched with respect to their capacity. It should be noted that Fig. 7(a) was generated by choosing a single module from the 130 modules simulated using the high manufacturing variation case and a single module from the 130 modules simulated from the low manufacturing variance case so that these two modules had the same capacity, an unlikely event that only occurs at the tail ends of their distributions. From Fig. 7(a), it is clear that as the manufacturing variance is increased, the minimum module voltage is also increased. This is because of the additive nature of the module voltage (Eq. 14) and the fact that manufacturing variations result in a spread of end-of-discharge voltages, as shown in Fig. 6(b). On average, over the 130 modules simulated for each manufacturing variation case, for low variance in manufacturing (as shown in Table 1), the modules cycle between high and low voltage limits of 63 V and 46.0 V $\pm$ 0.83 V whereas for the case of high variance in manufacturing, the modules cycle between 63 V and 49.8 V $\pm$ 0.86 V. It should be pointed out that the alogirthm used in this model ensures that the each cell within the module is fully charged to 4.2 V.

As has been previously mentioned, the battery module is limited by the cell that has the lowest capacity in the module. Fig. 7(b) shows the discharge profiles of the limiting cell within a module compared against the same cell but simulated as a single cell and not as part of a module. These two discharge curves are identical, however,Fig. 7(b) also shows the average discharge profile of all cells within the module, which takes on a slightly different shape to the limiting cell, again, caused by the distribution in cell voltages within a module. As a consequence of the higher average cell

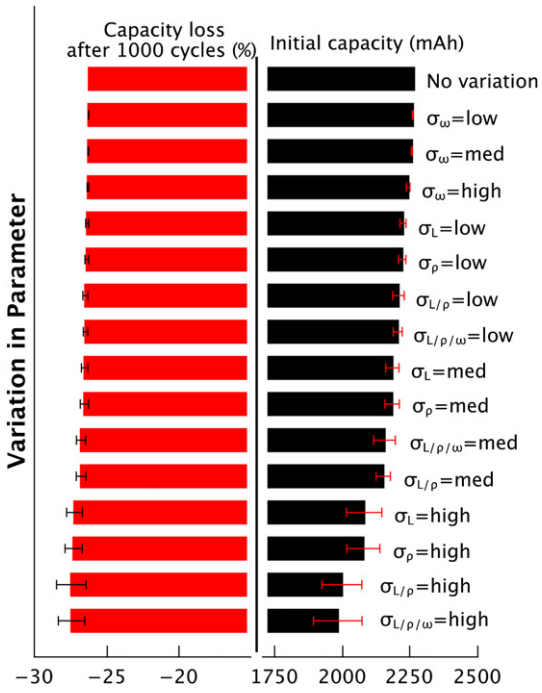

Fig. 9. (right) Initial capacity (at $I_{tot} = -0.8$ A) of a 15-cell lithium-ion battery module as a function of varying degrees of manufacturing tolerance. (L = electrode thickness, ρ = apparent electrode density, w = mass fraction of active material). (left) The capacity degradation (as a percentage of initial capacity) after 1000 cycles. The capacities represent the average of 130 simulations from randomly chosen parameters and the error bars represent the standard deviations.

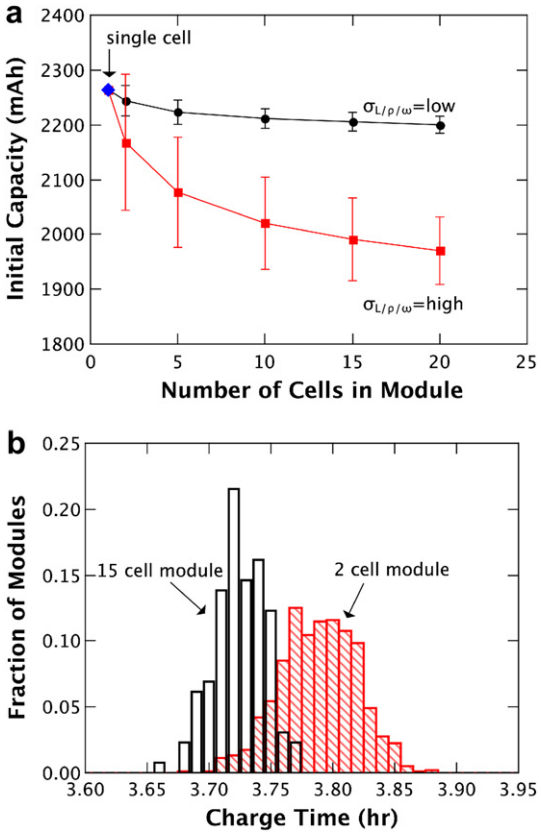

Fig. 10. (a) Initial capacity (at $I_{tot} = -0.8$ A) of a module as a function of the number of cells within the module for low and high manufacturing variations. The error bars represent the standard deviation of the capacities. (b) The distribution of charge times for modules assembled with 2 and 15 cells based on low manufacturing variations.

voltage caused by manufacturing variations, for two modules that have the same capacity but one module assembled from cells that have a wider variation in the single cell capacity, the total energy delivery for the module assembled with unbalanced cells is higher, due to the fact that the average cell voltage is higher. Again though, it should be emphasized that the probability of finding two modules with the same capacity made from both high and low manufacturing variation cells is low.

A common concern when it comes to lithium-ion batteries and battery packs is to estimate and to match the state-of-charge of cells within the battery pack. The state-of-charge and the shift in the state-of-charge with respect to cycle number can indicate the relative health of a battery system. Fig. 8(a) and (b) show the state-of-charge of the individual electrodes as a function of cycle time during the second cycle for the modules that exhibit the maximum variation in the state-of-charge (or in this case, lithiation of the electrodes) for modules assembled with cells made with low and high manufacturing variations. At the start of the cycle, the cells are fully charged due to the cell balancing algorithm that is commonly employed in battery management systems. During the discharge process, the state-of-charge of the cells begin to diverge due to small electrode microstructural differences introduced by the manufacturing stages that influence the kinetics and transport of lithium within the cells. The maximum state-of-charge mismatch occurs at the end-of-discharge and the extent of the mismatch is a function of the variation in the manufacturing of the cells. As can be see from the figures, the state-of-charge mismatch between cells made with low manufacturing variations is relatively minor but increases for cells made with high manufacturing variations. This mismatch in the state-of-charge of the cells indicates non-optimal utilization of each cell within the module and in some circumstances, may be difficult to correct for the battery management system.

From the above discussion, it is evident that battery modules assembled from cells that include even slight manufacturing variations can influence the distribution of cell-to-cell voltages and states-of-charge, resulting from the fact that electrochemical processes depend on the microstructure of the electrode. Although manufacturing variances of cells may result in some cells exhibiting higher capacities than the average, as shown in Fig. 5, modules are limited by the weakest cell within the module. For this reason, these distributions of cells within a battery module manifests itself in a lower module capacity. Fig. 9 shows the initial capacity and capacity fade of a 15-cell module for a systematic variation in manufacturing parameters from low to high variations as defined in Table 1. In this case, a hypothetical module built from cells that had identical electrode microstructures resulted in a module capacity of 2.26 Ah and a capacity fade of 26.2% after 1000 cycles whereas a module built from cells that had high manufacturing variations resulted in the lowest initial capacity of 1.99 Ah and a capacity fade of 27.4%. As the extent of variation in cell manufacturing increases, the capacity of the battery module decreased due to the fact that the probability of manufacturing a cell with a low capacity was higher. Interestingly though, as the extent of manufacturing variability increases, the capacity fade also increases. The reason for this slightly increased capacity fade was that the total side reaction current is a function of the electrode microstructure, based on Eq. 13a, and is therefore influenced by slight variations in the manufacturing of the electrodes. In addition, the result of the systematic variation in manufacturing parameters reveals that for the same level of variation in either the electrode thickness or the electrode's density, there is not a statistical

difference in the capacity of the module. However, between a 1% variation and a 2% variation in either of these manufacturing parameters, there is a statistical difference. This indicated that the electrode thickness and the electrode density are equally important to control during the manufacturing process of the cells wheareas the weight fraction of the electrode, as long as the variation is kept less than 0.5%, is less critical. The order of importance in the control of manufacturing can then be summarized as: $w_{AM} < \rho^{eode} \leq L$.

4.3.3. Variable sized modules

The above discussion has focused primarily on lithium-ion battery modules consisting of 15-cells configured in series. It is clear that the number of cells within a module could also influence the capacity of the module though, since the fewer cells there are in a module, the less likely it is that a low capacity cell would exist in that module. Fig. 10(a) shows the effect of the number of cells in a module on the initial capacity of the module for two cases of low and high manufacturing variations. The initial drop in the capacity when going from a single cell to a 2-cell module is initially steep, however, as is indicated by the error bars, depending on the extent of manufacturing variation, some modules could be made with limiting cells that have capacities higher than the target cell (in this case, a 2.26 Ah cell). The probability of assembling a module with all cells in the module having a high capacity is reduced as the number of cells in the module is increased and this results in the module capacity falling as the number of cells is increased. Fig. 10(a) shows that a 2-cell module made from cells with low manufacturing variation has a capacity of 2.24 ± 0.027 Ah whereas a 20-cell module has a capacity of 2.19 ± 0.016 Ah, a 1.9% drop in capacity. For high manufacturing variation, the drop in capacity caused by a shift from a 2-cell module to a 20-cell module is 9.1%.

Not surprisingly, the charge time for the modules also shifts as the number of cells in the module increase. Fig. 10(b) shows the distribution in the total charge time for each module simulated as with 2-cells and with 15-cells. The charging time for the 2-cell module is higher than that for a 15-cell module because in a 2-cell module, most of the capacity of each cell is used and therefore, must be more fully charged. Whereas in a 15-cell module, some cells do not discharge completely and therefore have a shorter charge time.

5. Conclusions

In this work, the single particle model for lithium-ion batteries was extended to simulate battery modules, or individual cells configured in series. The focus of the present study was to link the variation in the manufacturing of lithium-ion cells to the capacity of lithium-ion battery modules. Manufacturing variations following a normal distribution with a range of standard deviations were simulated. It was shown that the capacity of the module was limited by the weakest cell within the module, however, for modules assembled with cells made with high variations, the average voltage of the battery module may be higher which may result in higher energy delivery due to the fact that the module consists of some higher capacity cells in addition to lower capacity cells. Further, the study reaveals that the potential capacity of the cells in a battery module exceeds its active useful capacity, where the extent of capacity rendered unavailable is related to the degree of manufacturing variability at the individual cell level.

The simulations show that the initial capacity of a battery module is a strong function of manufacturing variations, but the capacity fade of the battery module also varies with the extent of manufacturing variations. In addition, the simulations suggest that two manufacturing parameters, the electrode thickness and the electrode's density (ie. porosity), are of equal and more significant importance to control in order to maximize the useful capacity of the battery module.

Acknowledgements

The authors would like to thank Natural Resources Canada for funding this work under the Program of Energy Research and Development (PERD).

References

[1] M. Doyle, T.F. Fuller, J. Newman, Journal of The Electrochemical Society 140 (1993) 1526–1533.
[2] M. Doyle, J. Newman, Electrochimica Acta 40 (1995) 2191–2196.
[3] M. Doyle, J. Newman, A.S. Gozdz, C.N. Schmutz, J.-M. Tarascon, Journal of The Electrochemical Society 143 (1996) 1890–1903.
[4] P. Arora, M. Doyle, A.S. Gozdz, R.E. White, J. Newman, Journal of Power Sources 88 (2000) 219–231.
[5] D.W. Dees, V.S. Battaglia, A. Blanger, Journal of Power Sources 110 (2002) 310–320.
[6] V. Srinivasan, J. Newman, Journal of The Electrochemical Society 151 (2004) A1517.
[7] V. Srinivasan, J. Newman, Journal of The Electrochemical Society 151 (2004) A1530–A1538.
[8] G. Ning, R. White, B. Popov, Electrochimica Acta 51 (2006) 2012–2022.
[9] S. Santhanagopalan, Q. Guo, P. Ramadass, R.E. White, Journal of Power Sources 156 (2006) 620–628.
[10] K. Kumaresan, G. Sikha, R.E. White, Journal of The Electrochemical Society 155 (2008) A164–A171.
[11] P. Ramadass, B. Haran, P.M. Gomadam, R.E. White, B.N. Popov, Journal of The Electrochemical Society 151 (2004) A196–A203.
[12] G. Ning, B.N. Popov, Journal of The Electrochemical Society 151 (2004) A1584–A1591.
[13] S.K. Rahimian, S.C. Rayman, R.E. White, Journal of, The Electrochemical Society 157 (2010) A1302.
[14] S.K. Rahimian, S. Rayman, R.E. White, Journal of Power Sources 196 (2011) 8450–8462.
[15] S.K. Rahimian, S. Rayman, R.E. White, Journal of Power Sources 196 (2011) 10297–10304.
[16] M. Guo, G. Sikha, R.E. White, Journal of The Electrochemical Society 158 (2011) A122–A132.
[17] A. Romero-Becerril, L. Alvarez-Icaza, Journal of Power Sources 196 (2011) 10267–10279.
[18] X. Hu, S. Li, H. Peng, Journal of Power Sources 198 (2011) 359–367.
[19] K. Smith, C.-Y. Wang, Journal of Power Sources 160 (2006) 662–673.
[20] C. Sen, N. Kar, 2009 IEEE Vehicle Power and Propulsion Conference (2009) 207–212.
[21] M. Dubarry, N. Vuillaume, B. Liaw, Journal of Power Sources 186 (2009) 500–507.
[22] L. Cai, R.E. White, Journal of Power Sources 196 (2011) 5985–5989.
[23] D.H. Jeon, S.M. Baek, Energy Conversion and Management 52 (2011) 2973–2981.
[24] A.M. Colclasure, K. a. Smith, R.J. Kee, Electrochimica Acta 58 (2011) 33–43.
[25] E. Jones, T. Oliphant, P. Peterson, et al., SciPy: Open Source Scientific Tools for Python (2001).http://www.scipy.org.
[26] B. Johnson, R. White, Journal of Power Sources 70 (1998) 48–54.
[27] F.M. Courtel, E. a. Baranova, Y. Abu-Lebdeh, I.J. Davidson, Journal of Power Sources 195 (2010) 2355–2361.
[28] H. Duncan, Y. Abu-Lebdeh, I.J. Davidson, Journal of The Electrochemical Society 157 (2010) A528.
[29] H. Duncan, D. Duguay, Y. Abu-Lebdeh, I.J. Davidson, Journal of The Electrochemical Society 158 (2011) A537.

Nomenclature

c: concentration of lithium in active material mol m^{-3}
D: diffusion coefficient m^2 s
J: intercalation current density A m^{-2}
J_s: side reaction current density A m^{-2}
i_0: exchange current density A m^{-2}
k_{ct}: rate constant of intercalation reaction m$^{2.5}$ s^{-1} mol$^{0.5}$
C_{max}: maximum lithium concentration in active material mol m^{-3}
C_e: concentration of lithium salt in electrolyte mol m^{-3}
E_{ref}: equilibrium potential V
R_{film}: resistance of SEI film on a surface area basis Ω m^2
M_p: molecular mass of side reaction product kg mol^{-1}
L_{SEI}: thickness of SEI film m
S_i: active internal surface area of electrode m^2
Q: capacity of electrode A s
V_i: volume fraction of either active material, binder or carbon filler –

w_i: weight fraction of either active material, binder or carbon filler −
R_p: radius of active material particle m^2
R: gas constant J mol^{-1} K^{-1}
T: temperature K
F: Farraday constant C mol^{-1}

Greek
θ_i: state-of-charge of electrode −
η_i: overpotential of charge of electrode V
$\phi_{1/2}$: electronic/ionic potential V
ρ_p: density of side reaction product kg m^{-3}
κ_p: conductivity of side reaction product S m^{-1}
ε: porosity of electrode −

Subscripts
i: positive or negative electrode
s: side reaction
j: active material, carbon filler or binder
ct: charge transfer reaction
P: product of the side reaction

Superscripts
eode: electrode
bulk: bulk electrode (ie. electrode without porosity)